



Measurement of isolated photon production in deep inelastic ep scattering

ZEUS Collaboration

S. Chekanov, M. Derrick, S. Magill, B. Musgrave, D. Nicholass¹, J. Repond, R. Yoshida

Argonne National Laboratory, Argonne, IL 60439-4815, USA²

M.C.K. Mattingly

Andrews University, Berrien Springs, MI 49104-0380, USA

P. Antonioli, G. Bari, L. Bellagamba, D. Boscherini, A. Bruni, G. Bruni, F. Cindolo, M. Corradi, G. Iacobucci, A. Margotti, R. Nania, A. Polini

INFN Bologna, Bologna, Italy³

S. Antonelli, M. Basile, M. Bindi, L. Cifarelli, A. Contin, S. De Pasquale⁴, G. Sartorelli, A. Zichichi

University and INFN Bologna, Bologna, Italy³

D. Bartsch, I. Brock, H. Hartmann, E. Hilger, H.-P. Jakob, M. Jüngst, A.E. Nuncio-Quiroz, E. Paul, U. Samson, V. Schönberg, R. Shehzadi, M. Wlasenko

Physikalisches Institut der Universität Bonn, Bonn, Germany⁵

J.D. Morris⁶

H.H. Wills Physics Laboratory, University of Bristol, Bristol, United Kingdom⁷

M. Kaur, P. Kaur⁸, I. Singh⁸

Panjab University, Department of Physics, Chandigarh, India

M. Capua, S. Fazio, A. Mastroberardino, M. Schioppa, G. Susinno, E. Tassi⁹

Calabria University Physics Department and INFN, Cosenza, Italy³

Chonnam National University, Kwangju, South Korea

Z.A. Ibrahim, F. Mohamad Idris, B. Kamaluddin, W.A.T. Wan Abdullah

Jabatan Fizik, Universiti Malaya, 50603 Kuala Lumpur, Malaysia¹¹

Y. Ning, Z. Ren, F. Sciulli

Nevis Laboratories, Columbia University, Irvington on Hudson, NY 10027, USA¹²

J. Chwastowski, A. Eskreys, J. Figiel, A. Galas, K. Olkiewicz, B. Pawlik, P. Stopa, L. Zawiejski

The Henryk Niewodniczanski Institute of Nuclear Physics, Polish Academy of Sciences, Cracow, Poland¹³

L. Adamczyk, T. Bołd, I. Grabowska-Bołd, D. Kisielewska, J. Łukasik¹⁴, M. Przybycień, L. Suszycki

Faculty of Physics and Applied Computer Science, AGH-University of Science and Technology, Cracow, Poland¹⁵

A. Kotański¹⁶, W. Słomiński¹⁷

Department of Physics, Jagellonian University, Cracow, Poland

O. Bachynska, O. Behnke, J. Behr, U. Behrens, C. Blohm, K. Borrás, D. Bot, R. Ciesielski, N. Coppola, S. Fang, A. Geiser, P. Göttlicher¹⁸, J. Grebenyuk, I. Gregor, T. Haas*, W. Hain, A. Hüttmann, F. Januschek, B. Kahle, I.I. Katkov¹⁹, U. Klein²⁰, U. Kötz, H. Kowalski, V. Libov, M. Lisovyi, E. Lobodzinska, B. Löhr, R. Mankel²¹, I.-A. Melzer-Pellmann, S. Miglioranza²², A. Montanari, T. Namsou, D. Notz, A. Parenti, P. Roloff, I. Rubinsky, U. Schneekloth, A. Spiridonov²³, D. Szuba²⁴, J. Szuba²⁵, T. Theedt, J. Tomaszewska²⁶, G. Wolf, K. Wrona, A.G. Yagües-Molina, C. Youngman, W. Zeuner²¹

Deutsches Elektronen-Synchrotron DESY, Hamburg, Germany

V. Drugakov, W. Lohmann, S. Schlenstedt

Deutsches Elektronen-Synchrotron DESY, Zeuthen, Germany

G. Barbagli, E. Gallo

INFN Florence, Florence, Italy³

P.G. Pelfer

University and INFN Florence, Florence, Italy³

A. Bamberger, D. Dobur, F. Karstens, N.N. Vlasov²⁷

Fakultät für Physik der Universität Freiburg i.Br., Freiburg i.Br., Germany⁵

P.J. Bussey, A.T. Doyle, M. Forrest, D.H. Saxon, I.O. Skillicorn

Department of Physics and Astronomy, University of Glasgow, Glasgow, United Kingdom⁷

I. Gialas²⁸, K. Papageorgiu

Department of Engineering in Management and Finance, Univ. of the Aegean, Chios, Greece

U. Holm, R. Klanner, E. Lohrmann, H. Perrey, P. Schleper, T. Schörner-Sadenius, J. Sztuk, H. Stadie, M. Turcato

Hamburg University, Institute of Exp. Physics, Hamburg, Germany⁵

K.R. Long, A.D. Tapper

Imperial College London, High Energy Nuclear Physics Group, London, United Kingdom⁷

T. Matsumoto²⁹, K. Nagano, K. Tokushuku³⁰, S. Yamada, Y. Yamazaki³¹

Institute of Particle and Nuclear Studies, KEK, Tsukuba, Japan³²

A.N. Barakbaev, E.G. Boos, N.S. Pokrovskiy, B.O. Zhautykov

Institute of Physics and Technology of Ministry of Education and Science of Kazakhstan, Almaty, Kazakhstan

V. Aushev³³, M. Borodin, I. Kadenko, Ie. Korol, O. Kuprash, D. Lontkovskiy, I. Makarenko, Yu. Onishchuk, A. Saliı, Iu. Sorokin, A. Verbytskyi, V. Viazlo, O. Volynets, O. Zenaiev, M. Zolko

Institute for Nuclear Research, National Academy of Sciences, and Kiev National University, Kiev, Ukraine

D. Son

Kyungpook National University, Center for High Energy Physics, Daegu, South Korea³⁴

J. de Favereau, K. Piotrkowski

*Institut de Physique Nucléaire, Université Catholique de Louvain, Louvain-la-Neuve, Belgium*³⁵

F. Barreiro, C. Glasman, M. Jimenez, J. del Peso, E. Ron, J. Terrón, C. Uribe-Estrada

*Departamento de Física Teórica, Universidad Autónoma de Madrid, Madrid, Spain*³⁶

F. Corriveau, J. Schwartz, C. Zhou

*Department of Physics, McGill University, Montréal, Québec, Canada H3A 2T8*³⁷

T. Tsurugai

*Meiji Gakuin University, Faculty of General Education, Yokohama, Japan*³²

A. Antonov, B.A. Dolgoshein, D. Gladkov, V. Sosnovtsev, A. Stifutkin, S. Suchkov

*Moscow Engineering Physics Institute, Moscow, Russia*³⁸

R.K. Dementiev, P.F. Ermolov³⁹, L.K. Gladilin, Yu.A. Golubkov, L.A. Khein, I.A. Korzhavina, V.A. Kuzmin, B.B. Levchenko⁴⁰, O.Yu. Lukina, A.S. Proskuryakov, L.M. Shcheglova, D.S. Zotkin

*Moscow State University, Institute of Nuclear Physics, Moscow, Russia*⁴¹

I. Abt, A. Caldwell, D. Kollar, B. Reiser, W.B. Schmidke

Max-Planck-Institut für Physik, München, Germany

G. Grigorescu, A. Keramidas, E. Koffeman, P. Kooijman, A. Pellegrino, H. Tiecke, M. Vázquez²², L. Wiggers

*NIKHEF and University of Amsterdam, Amsterdam, The Netherlands*⁴²

N. Brümmer, B. Bylsma, L.S. Durkin, A. Lee, T.Y. Ling

*Physics Department, Ohio State University, Columbus, OH 43210, USA*²

A.M. Cooper-Sarkar, R.C.E. Devenish, J. Ferrando, B. Foster, C. Gwenlan⁴³, K. Horton⁴⁴, K. Oliver, A. Robertson, R. Walczak

*Department of Physics, University of Oxford, Oxford, United Kingdom*⁷

A. Bertolin, F. Dal Corso, S. Dusini, A. Longhin, L. Stanco

*INFN Padova, Padova, Italy*³

R. Brugnera, R. Carlin, A. Garfagnini, S. Limentani

*Dipartimento di Fisica dell'Università and INFN, Padova, Italy*³

B.Y. Oh, A. Raval, J.J. Whitmore⁴⁵

*Department of Physics, Pennsylvania State University, University Park, PA 16802, USA*¹²

Y. Iga

*Polytechnic University, Sagamihara, Japan*³²

G. D'Agostini, G. Marini, A. Nigro

*Dipartimento di Fisica, Università La Sapienza' and INFN, Rome, Italy*³

J.C. Hart

*Rutherford Appleton Laboratory, Chilton, Didcot, Oxon, United Kingdom*⁷

H. Abramowicz⁴⁶, R. Ingbir, S. Kananov, A. Levy, A. Stern

Raymond and Beverly Sackler Faculty of Exact Sciences, School of Physics, Tel Aviv University, Tel Aviv, Israel⁴⁷

M. Ishitsuka, T. Kanno, M. Kuze, J. Maeda

Department of Physics, Tokyo Institute of Technology, Tokyo, Japan³²

R. Hori, N. Okazaki, S. Shimizu²²

Department of Physics, University of Tokyo, Tokyo, Japan³²

R. Hamatsu, S. Kitamura⁴⁸, O. Ota⁴⁹, Y.D. Ri⁵⁰

Tokyo Metropolitan University, Department of Physics, Tokyo, Japan³²

M. Costa, M.I. Ferrero, V. Monaco, R. Sacchi, V. Sola, A. Solano

Università di Torino and INFN, Torino, Italy³

M. Arneodo, M. Ruspa

Università del Piemonte Orientale, Novara, and INFN, Torino, Italy³

S. Fourletov⁵¹, J.F. Martin, T.P. Stewart

Department of Physics, University of Toronto, Toronto, Ontario, Canada M5S 1A7³⁷

S.K. Boutle²⁸, J.M. Butterworth, T.W. Jones, J.H. Loizides, M. Wing

Physics and Astronomy Department, University College London, London, United Kingdom⁷

B. Brzozowska, J. Ciborowski⁵², G. Grzelak, P. Kulinski, P. Łuzniak⁵³, J. Malka⁵³, R.J. Nowak, J.M. Pawlak, W. Perlanski⁵³, A.F. Żarnecki

Warsaw University, Institute of Experimental Physics, Warsaw, Poland

M. Adamus, P. Plucinski⁵⁴, T. Tymieniecka⁵⁵

Institute for Nuclear Studies, Warsaw, Poland

Y. Eisenberg, D. Hochman, U. Karshon

Department of Particle Physics, Weizmann Institute, Rehovot, Israel⁵⁶

E. Brownson, D.D. Reeder, A.A. Savin, W.H. Smith, H. Wolfe

Department of Physics, University of Wisconsin, Madison, WI 53706, USA²

S. Bhadra, C.D. Catterall, G. Hartner, U. Noor, J. Whyte

Department of Physics, York University, Ontario, Canada M3J 1P3³⁷

ARTICLE INFO

Article history:

Received 26 October 2009
 Received in revised form 29 January 2010
 Accepted 18 February 2010
 Available online 20 February 2010
 Editor: L. Rolandi

Keywords:

DIS
 Photon emission
 Quark radiation
 Isolated photon

ABSTRACT

Isolated photon production in deep inelastic ep scattering has been measured with the ZEUS detector at HERA using an integrated luminosity of 320 pb^{-1} . Measurements were made in the isolated-photon transverse-energy and pseudorapidity ranges $4 < E_T^\gamma < 15 \text{ GeV}$ and $-0.7 < \eta^\gamma < 0.9$ for exchanged photon virtualities, Q^2 , in the range $10 < Q^2 < 350 \text{ GeV}^2$ and for invariant masses of the hadronic system $W_X > 5 \text{ GeV}$. Differential cross sections are presented for inclusive isolated photon production as functions of Q^2 , x , E_T^γ and η^γ . Leading-logarithm parton-shower Monte Carlo simulations and perturbative QCD predictions give a reasonable description of the data over most of the kinematic range.

© 2010 Elsevier B.V. Open access under [CC BY license](#).

1. Introduction

In the study of high-energy collisions involving hadrons, events in which an isolated high-energy photon is observed provide a direct probe of the underlying partonic process, since the emission of these photons is unaffected by parton hadronisation.

* Corresponding author.

E-mail address: tobias.haas@desy.de (T. Haas).

- ¹ Also affiliated with University College London, United Kingdom.
- ² Supported by the US Department of Energy.
- ³ Supported by the Italian National Institute for Nuclear Physics (INFN).
- ⁴ Now at University of Salerno, Italy.
- ⁵ Supported by the German Federal Ministry for Education and Research (BMBF), under contract Nos. 05 HZ6PDA, 05 HZ6GUA, 05 HZ6VFA and 05 HZ4KHA.
- ⁶ Now at Queen Mary University of London, United Kingdom.
- ⁷ Supported by the Science and Technology Facilities Council, UK.
- ⁸ Also working at Max Planck Institute, Munich, Germany.
- ⁹ Also Senior Alexander von Humboldt Research Fellow at Hamburg University, Institute of Experimental Physics, Hamburg, Germany.
- ¹⁰ Supported by Chonnam National University, South Korea, in 2009.
- ¹¹ Supported by an FRGS grant from the Malaysian government.
- ¹² Supported by the US National Science Foundation. Any opinion, findings and conclusions or recommendations expressed in this material are those of the authors and do not necessarily reflect the views of the National Science Foundation.
- ¹³ Supported by the Polish State Committee for Scientific Research, project No. DESY/256/2006 - 154/DES/2006/03.
- ¹⁴ Now at Institute of Aviation, Warsaw, Poland.
- ¹⁵ Supported by the Polish Ministry of Science and Higher Education as a scientific project (2009–2010).
- ¹⁶ Supported by the research grant No. 1 P03B 04529 (2005–2008).
- ¹⁷ This work was supported in part by the Marie Curie Actions Transfer of Knowledge project COCOS (contract MTKD-CT-2004-517186).
- ¹⁸ Now at DESY group FEB, Hamburg, Germany.
- ¹⁹ Also at Moscow State University, Russia.
- ²⁰ Now at University of Liverpool, United Kingdom.
- ²¹ On leave of absence at CERN, Geneva, Switzerland.
- ²² Now at CERN, Geneva, Switzerland.
- ²³ Also at Institute of Theoretical and Experimental Physics, Moscow, Russia.
- ²⁴ Also at INP, Cracow, Poland.
- ²⁵ Also at FPACS, AGH-UST, Cracow, Poland.
- ²⁶ Partially supported by Warsaw University, Poland.
- ²⁷ Partially supported by Moscow State University, Russia.
- ²⁸ Also affiliated with DESY, Germany.
- ²⁹ Now at Japan Synchrotron Radiation Research Institute (JASRI), Hyogo, Japan.
- ³⁰ Also at University of Tokyo, Japan.
- ³¹ Now at Kobe University, Japan.
- ³² Supported by the Japanese Ministry of Education, Culture, Sports, Science and Technology (MEXT) and its grants for Scientific Research.
- ³³ Supported by DESY, Germany.
- ³⁴ Supported by the Korean Ministry of Education and Korea Science and Engineering Foundation.
- ³⁵ Supported by FNRS and its associated funds (IISN and FRIA) and by an Inter-University Attraction Poles Programme subsidised by the Belgian Federal Science Policy Office.
- ³⁶ Supported by the Spanish Ministry of Education and Science through funds provided by CICYT.
- ³⁷ Supported by the Natural Sciences and Engineering Research Council of Canada (NSERC).
- ³⁸ Partially supported by the German Federal Ministry for Education and Research (BMBF).
- ³⁹ Deceased.
- ⁴⁰ Partially supported by Russian Foundation for Basic Research grant No. 05-02-39028-NSFC-a.
- ⁴¹ Supported by RF Presidential grant N 1456.2008.2 for the leading scientific schools and by the Russian Ministry of Education and Science through its grant for Scientific Research on High Energy Physics.
- ⁴² Supported by the Netherlands Foundation for Research on Matter (FOM).
- ⁴³ STFC Advanced Fellow.
- ⁴⁴ Nee Korcsak-Gorzo.
- ⁴⁵ This material was based on work supported by the National Science Foundation, while working at the Foundation.

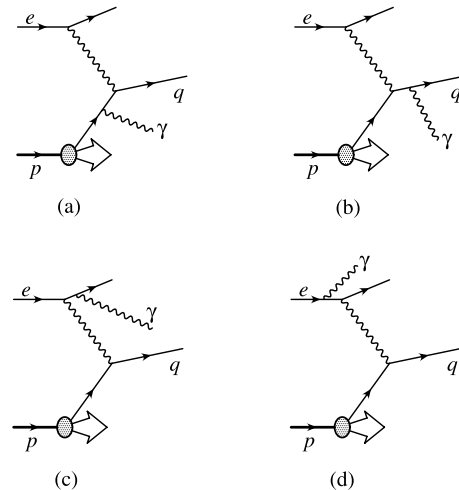


Fig. 1. Lowest-order tree-level diagrams for isolated photon production in ep scattering.

Isolated high-energy photon production has been studied in a number of fixed-target and hadron-collider experiments [1]. Previous ZEUS and H1 publications have also reported the production of isolated photons in photoproduction [$Q^2 \approx 0$], and deep inelastic scattering (DIS) [7,8], in which $Q^2 \approx \text{GeV}^2$.

Isolated photons are produced in DIS at lowest order in QCD as shown in Fig. 1. Photons produced by radiation from an incoming or outgoing quark are called “prompt”; an additional class of high-energy photons comprises those radiated from the incoming or outgoing lepton. In this Letter, results are presented from a new inclusive measurement of isolated photon production in neutral current DIS. The data provide a test of perturbative QCD in a kinematic region with two hard scales: Q^2 , the exchanged photon virtuality, and E_T^γ , the transverse energy of the emitted photon. Compared to the previous ZEUS publication [7], the kinematic reach extends to lower values of Q^2 and to higher values of E_T^γ . The statistical precision is also improved.

Leading-logarithm parton-shower Monte Carlo (MC) and perturbative QCD predictions are compared to the measurements. The cross sections for isolated photon production in DIS have been calculated to order $O(\alpha^3)$ by Gehrmann-De Ridder et al. (GGP) [9–11]. A calculation based on QED contributions to the parton distributions has been made by Martin et al. (MRST) [12].

2. Experimental set-up

The measurements are based on a data sample corresponding to an integrated luminosity of $320 \pm 8 \text{ pb}^{-1}$, taken between 2004 and 2007 with the ZEUS detector at HERA. The sample is a sum of

- ⁴⁶ ALSO at Max Planck Institute, Munich, Germany, Alexander von Humboldt Research Award.
- ⁴⁷ Supported by the Israel Science Foundation.
- ⁴⁸ Now at Nihon Institute of Medical Science, Japan.
- ⁴⁹ Now at SunMelx Co. Ltd., Tokyo, Japan.
- ⁵⁰ Now at Osaka University, Osaka, Japan.
- ⁵¹ Now at University of Bonn, Germany.
- ⁵² Also at Łódź University, Poland.
- ⁵³ Member of Łódź University, Poland.
- ⁵⁴ Now at Lund University, Lund, Sweden.
- ⁵⁵ Also at University of Podlasie, Siedlce, Poland.
- ⁵⁶ Supported in part by the MINERVA Gesellschaft für Forschung GmbH, the Israel Science Foundation (grant No. 293/02-11.2) and the US–Israel Binational Science Foundation.

$131 \pm 3 \text{ pb}^{-1}$ of e^+p data and $189 \pm 5 \text{ pb}^{-1}$ of e^-p data⁵⁷ with centre-of-mass energy $\sqrt{s} = 318 \text{ GeV}$.

A detailed description of the ZEUS detector can be found elsewhere [13]. Charged particles were tracked in the central tracking detector (CTD) [14] and a silicon micro vertex detector (MVD) [15] which operated in a magnetic field of 1.43 T provided by a thin superconducting solenoid. The high-resolution uranium-scintillator calorimeter (CAL) [16] consisted of three parts: the forward (FCAL), the barrel (BCAL) and the rear (RCAL) calorimeters. The BCAL covers the pseudorapidity range -0.74 to 1.01 as seen from the nominal interaction point. The FCAL and RCAL extend the range to -3.5 to 4.0 . The smallest subdivision of the CAL was called a cell. The barrel electromagnetic calorimeter (BEMC) cells had a pointing geometry aimed at the nominal interaction point, with a cross section approximately $5 \times 20 \text{ cm}^2$, with the finer granularity in the Z-direction.⁵⁸ This fine granularity allows the use of shower-shape distributions to distinguish isolated photons from the products of neutral meson decays such as $\pi^0 \rightarrow \gamma\gamma$.

A three-level trigger system was used to select events online [17] by requiring well isolated electromagnetic deposits in the CAL.

The luminosity was measured using the Bethe–Heitler reaction $ep \rightarrow e\gamma p$ by a luminosity detector which consisted of two independent systems: a lead-scintillator calorimeter [18] and a magnetic spectrometer [19].

3. Event selection and reconstruction

Events were selected offline by requiring a scattered-electron candidate, identified using a neural network [20]. The candidates were required to have a polar angle in the range $139.8^\circ < \theta_e < 171.9^\circ$ in order to ensure that they were well measured in the RCAL. The impact point (X, Y) of the candidate on the surface of the RCAL was required to lie outside the region $(\pm 15 \text{ cm}, \pm 15 \text{ cm})$ centred on $(0, 0)$ to ensure well understood acceptance. The energy of the candidate, E'_e , was required to be larger than 10 GeV . The kinematic quantities Q^2 and x were reconstructed from the scattered electron by means of the relationships $Q^2 = -(k - k')^2$ and $x = Q^2 / (2P \cdot (k - k'))$ where k (k') is the four-momentum of the incoming (outgoing) lepton and P is the four-momentum of the incoming proton. The kinematic region $10 < Q^2 < 350 \text{ GeV}^2$ was selected.

To reduce backgrounds from non- ep collisions, events were required to have a reconstructed vertex position, Z_{vtx} , within the range $|Z_{\text{vtx}}| < 40 \text{ cm}$ and to have $35 < \delta < 65 \text{ GeV}$, where $\delta = \sum_i E_i (1 - \cos \theta_i)$; E_i is the energy of the i th CAL cell, θ_i is its polar angle and the sum runs over all cells [21]. At least one reconstructed track, well separated from the electron, was required, ensuring some hadronic activity which suppressed deeply virtual Compton scattering (DVCS) [22] to a negligible level.

Photon candidates were identified as CAL energy-flow objects (EFOs) [23] for which at least 90% of the reconstructed energy was measured in the BEMC. EFOs with wider electromagnetic showers than are typical of a single photon were accepted to allow evaluation of backgrounds. The reconstructed transverse energy of the EFO, E_T^γ , was required to lie within the range $4 < E_T^\gamma < 15 \text{ GeV}$ and the pseudorapidity, η^γ , had to satisfy $-0.7 < \eta^\gamma < 0.9$. The upper limit on the reconstructed transverse energy was selected to en-

sure that the shower shapes from background and signal remained distinguishable.

To reduce the background from photons and neutral mesons within jets, the EFO was required to be isolated from reconstructed tracks and hadronic activity. Isolation from tracks was initially achieved by demanding $\Delta R > 0.2$, where $\Delta R = \sqrt{(\Delta\phi)^2 + (\Delta\eta)^2}$ is the distance to the nearest reconstructed track with momentum greater than 250 MeV in the η - ϕ plane, where ϕ is the azimuthal angle. Jet reconstruction was performed on all EFOs in the event, including the electron and photon candidates, using the k_T cluster algorithm [24] in the longitudinally invariant inclusive mode [25] with R parameter set to 1.0 . Further isolation was imposed by requiring that the photon-candidate EFO possessed at least 90% of the total energy of the jet of which it formed a part.

Each event was required to contain both an electron and a photon candidate. The invariant mass of the hadronic system, W_X , is then defined by $W_X^2 = (P + k - k' - p_\gamma)^2$, where p_γ is the four-vector of the outgoing photon. A total of 15 699 events were selected; at this stage the sample was dominated by background events. The largest source of background was neutral current (NC) DIS events where a genuine electron candidate was found in the RCAL and neutral mesons, such as π^0 and η , decaying to photons, produced a photon-candidate EFO in the BEMC.

4. Theory

Two theoretical predictions are compared to the measurements presented in this Letter. In the approach of GGP [10], the contributions to the scattering cross section for $ep \rightarrow e\gamma X$ are calculated at order α^3 in the electromagnetic coupling. One of these contributions comes from the radiation of a photon from the quark line (called QQ photons; Fig. 1a, b) and a second from the radiation from the lepton line (called LL photons; Fig. 1c, d). In addition to QQ and LL photons, the interference term between photon emission from the lepton and quark lines, called LQ photons by GGP, is evaluated. For the kinematic region considered here, where the outgoing photon is well separated from both outgoing electron and quark, the interference term gives only a 3% effect on the cross section. This effect is further reduced to $\approx 1\%$ when e^+p and e^-p data are combined as the LQ term changes sign when e^- is replaced by e^+ . The QQ contribution includes both wide-angle photon emission and the leading $q \rightarrow q\gamma$ fragmentation term. GGP have chosen to use CTEQ6L leading-order parton distribution functions [26]. The factorisation scales used are Q for QQ events and $\max(Q, \mu_{F,\min})$ for LL events where $\mu_{F,\min} = 1 \text{ GeV}$. Parton-to-hadron corrections were not made, in view of technical issues in relating $2 \rightarrow 2$ and $2 \rightarrow 3$ topologies, following the advice of the GGP authors. We note that others have taken a different view [8]. A naïve study indicated the likely effect to be a reduction after hadronisation in predicted inclusive cross-sections of order 15%.

In the approach of MRST [12,27], a partonic photon component of the proton, γ_p , is introduced as a consequence of including QED corrections in the parton distribution functions. This leads to ep interactions taking place via QED Compton scattering, $\gamma_p e \rightarrow \gamma e$. A measurement of the isolated high-energy photon production cross section therefore provides a constraint on the photon density in the proton. The model includes the collinearly divergent LL contribution, which is enhanced relative to that of GGP by the DGLAP resummation due to the inclusion of QED Compton scattering. The QQ component is not included in the MRST model, in which the transverse momentum of the scattered electron is expected to balance approximately that of the isolated photon. In the analysis presented here, such a constraint was not imposed. The theoretical uncertainties in the models have been estimated by varying the factorisation scales by a factor two.

⁵⁷ Hereafter ‘electron’ refers to both electrons and positrons unless otherwise specified.

⁵⁸ The ZEUS coordinate system is a right-handed Cartesian system, with the Z axis pointing in the proton beam direction, referred to as the ‘forward direction’, and the X axis pointing towards the centre of HERA. The coordinate origin is at the nominal interaction point.

Since the MRST cross sections include the LL contribution of GGP to a good approximation, but exclude the QQ, an improved prediction can be constructed by summing the MRST cross section and the QQ cross section from GGP [27,28]. The theory uncertainties are of the same order as those of the individual QQ and LL components.

5. Monte Carlo event simulation

The MC program PYTHIA 6.416 [29] was used to simulate prompt-photon emission for the study of the event-reconstruction efficiency. In PYTHIA, this process is simulated as a DIS process with additional photon radiation from the quark line to account for QQ photons. Radiation from the lepton is not simulated in this PYTHIA sample.

The LL photons radiated at large angles from the incoming or outgoing electron were simulated using the generator DJANGO 6 [30], an interface to the MC program HERACLES 4.6.6 [31]; higher-order QCD effects were included using the colour dipole model of ARIADNE 4.12 [32]. Hadronisation of the partonic final state was performed by JETSET 7.4 [33]. The small LQ contribution was neglected.

The NC DIS background was simulated using DJANGO 6, within the same framework as the LL events. This provided a realistic spectrum of mesons and overlapping clusters with well modelled kinematic distributions and hence was preferred to single-particle MC samples for backgrounds, such as were used in the previous ZEUS publication [7].

The MC samples described above contained only events in which W_X was larger than 5 GeV. Isolated photons can also be produced at values of W_X less than 5 GeV in ‘elastic’ and ‘quasi-elastic’ processes ($ep \rightarrow ep\gamma$) such as DVCS and Bethe–Heitler photon production. Such events were simulated using the GENDVCS [34] and GRAPE-COMPTON [35] generators. The contribution of these elastic processes was negligible after the selections described in Section 3.

The generated MC events were passed through the ZEUS detector and trigger simulation programs based on GEANT 3.21 [36]. They were reconstructed and analysed by the same programs as the data. In addition to the full-event simulations, MC samples of single particles (photons and neutral mesons) were generated and used to study the MC description of electromagnetic showering in the BEMC.

6. Extraction of the photon signal

The event sample selected according to the criteria in Section 3 was dominated by background; thus the photon signal was extracted statistically following the approach used in previous ZEUS analyses [2–4,7].

The photon signal was extracted from the background using BEMC energy-cluster shapes. Two shape variables were considered:

- the variable $\langle \delta Z \rangle = \frac{\sum_i E_i |Z_i - Z_{\text{cluster}}|}{w_{\text{cell}} \sum_i E_i}$, where Z_i is the Z position of the centre of the i th cell, Z_{cluster} is the centroid of the EFO cluster, w_{cell} is the width of the cell in the Z direction, E_i is the energy recorded in the cell and the sum runs over all BEMC cells in the EFO;
- the ratio f_{max} of the highest energy deposited in any one BEMC cell in the EFO to the total EFO BEMC energy.

The distributions of $\langle \delta Z \rangle$ and f_{max} (after the requirement $\langle \delta Z \rangle < 0.8$) in the data and the MC are shown in Fig. 2. The MC LL and QQ distributions have been corrected in each two-dimensional

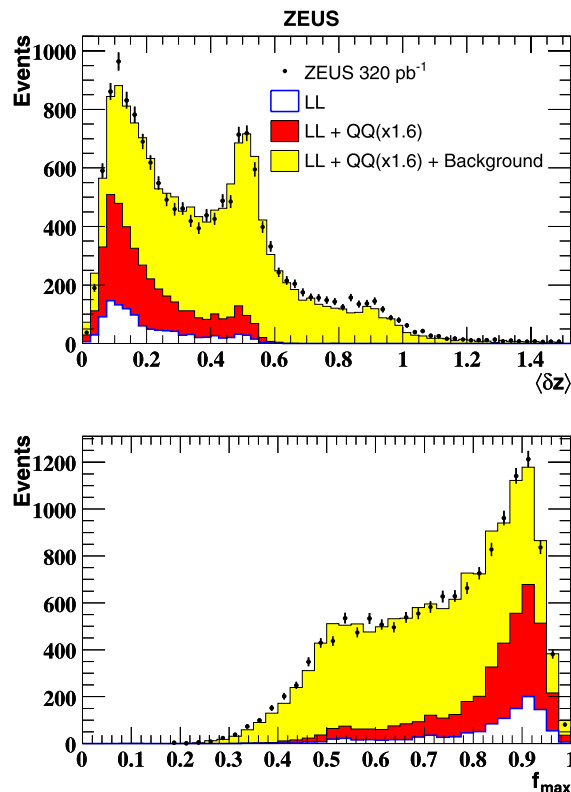


Fig. 2. Distributions of $\langle \delta Z \rangle$ and f_{max} . The error bars represent the statistical uncertainties. The light shaded histogram shows a fit to the data of three components with fixed shapes as described in the text. The dark shaded histogram represents the QQ component of the fit, and the white histogram the LL component. The f_{max} distribution is shown after requiring $\langle \delta Z \rangle < 0.8$.

(η , E_T) bin using factors derived from the difference between simulated and real DIS electron data. The $\langle \delta Z \rangle$ distribution exhibits a double-peaked structure with the first peak at ≈ 0.1 , associated with the signal, and a second peak at ≈ 0.5 , dominated by the $\pi^0 \rightarrow \gamma\gamma$ background. The f_{max} distribution shows a single peak at ≈ 0.9 corresponding to the photon signal, and has a shoulder extending down to ≈ 0.5 , which is dominated by the hadronic background.

The number of isolated-photon events contributing to Fig. 2 and in each cross-section bin was determined by a χ^2 fit to the $\langle \delta Z \rangle$ distribution in the range $0 < \langle \delta Z \rangle < 0.8$ using the LL and QQ signal and background MC distributions as described in Section 5. By treating the LL and QQ photons separately, one automatically takes account of their differing hadronic activity (resulting in significantly different acceptances) and their differing (η , E_T) distributions (resulting in different bin migrations due to finite measuring precision).

In performing the fit, the LL contribution was kept constant at its MC-predicted value and the other components were varied. Of the 15 699 events selected, 4164 ± 168 correspond to the extracted signal (LL and QQ). The scale factor resulting from the global fit for the QQ photons in Fig. 2 was 1.6; this factor was used for all the plots comparing MC to data. The fitted global scale factor for the hadronic background was 1.0. The signal fraction in the cross-section bins varied from 21% to 62%. In all cross-section bins, the $\chi^2/\text{n.d.f.}$ of the fits was 2.1 or smaller.

For a given observable Y , the production cross section was determined using:

$$\frac{d\sigma}{dY} = \frac{A_{\text{QQ}} \cdot N(\gamma_{\text{QQ}})}{\mathcal{L} \cdot \Delta Y} + \frac{d\sigma_{\text{LL}}^{\text{MC}}}{dY},$$

where $N(\gamma_{\text{QQ}})$ is the number of QQ photons extracted from the fit, ΔY is the bin width, \mathcal{L} is the total integrated luminosity, $\sigma_{\text{LL}}^{\text{MC}}$ is the predicted cross section for LL photons from DJANGO, and \mathcal{A}_{QQ} is the acceptance correction for QQ photons. The value of \mathcal{A}_{QQ} was calculated using Monte Carlo from the ratio of the number of events generated to those reconstructed in a given bin. It varied between 1.2 and 1.7 from bin to bin.

The fits employed in this analysis were performed using $\langle\delta Z\rangle$ because of the larger difference in shape between signal and background for this quantity. Fits in terms of the f_{max} distributions were performed as a cross-check and gave similar results. As a further cross-check, an algorithm from the previous ZEUS publication [7], which selects wider electromagnetic clusters as photon candidates, was used. This proved to be more sensitive to the modelling of calorimeter backgrounds. In every case where a satisfactory fit was obtained, good agreement with the principal method was found. The corrections to the MC photon-signal energy-cluster shapes gave changes to the results within the statistical uncertainties and were not further considered [37].

7. Systematic uncertainties

The following sources of systematic uncertainty were investigated [37]:

- the energy scale of the electromagnetic calorimeter (EMC) was varied by its known scale uncertainty of $\pm 2\%$ causing variations in the measured cross sections of typically less than $\pm 2\%$;
- the dependence on the modelling of the hadronic background by ARIADNE was investigated by varying the upper limit for the $\langle\delta Z\rangle$ fit in the range 0.6–1.0, giving variations that were typically $\pm 5\%$ but up to $+12\%$ and -14% in the most forward η^γ and highest- x bins respectively.

The following sources of systematic uncertainty were also investigated and found to be negligible compared to the statistical uncertainty [37]:

- variation of the EMC energy-fraction cut for the photon candidate EFO by $\pm 5\%$;
- variation of the Z_{vtx} cut by ± 5 cm;
- variation of the upper and lower cuts on δ by ± 3 GeV;
- variation of the ΔR cut used for track isolation by ± 0.1 ;
- variation of the track-momentum cut used in calculating track isolation by ± 100 MeV;
- variation of the LL-signal component by $\pm 5\%$.

All the uncertainties listed above were added in quadrature to give separate positive and negative systematic uncertainties in each bin. The uncertainty of 2.6% on the luminosity measurement was not included in the differential cross sections but included in the integrated cross sections.

8. Results

The cross section for inclusive isolated photon production, $ep \rightarrow e\gamma X$, was measured in the kinematic region defined by: $10 < Q^2 < 350 \text{ GeV}^2$, $W_X > 5 \text{ GeV}$, $E_e' > 10 \text{ GeV}$, $139.8^\circ < \theta_e < 171.8^\circ$, $-0.7 < \eta^\gamma < 0.9$ and $4 < E_T^\gamma < 15 \text{ GeV}$, with isolation such that at least 90% of the energy of the jet containing the photon belongs to the photon, where jets were formed according to the k_T algorithm with R parameter set 1.0. The measured integrated cross section is

$$19.4 \pm 0.7 \text{ (stat.)}_{-1.0}^{+1.2} \text{ (syst.) pb,}$$

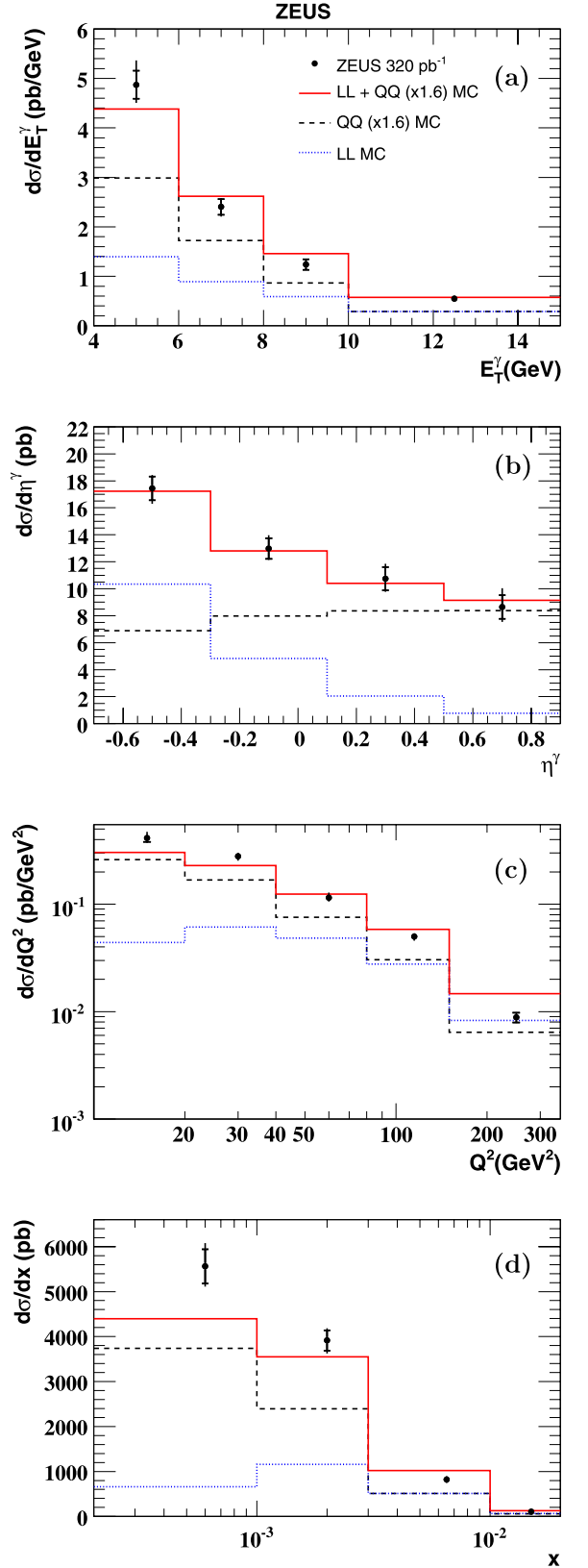


Fig. 3. Isolated photon differential cross sections in (a) E_T^γ , (b) η^γ , (c) Q^2 and (d) x . The inner and outer error bars show, respectively, the statistical uncertainty and the statistical and systematic uncertainties added in quadrature. The solid histograms are the Monte Carlo predictions from the sum of QQ photons from PYTHIA normalised by a factor 1.6 plus DJANGO LL photons. The dashed (dotted) lines show the QQ (LL) contributions.

Table 1Measured differential cross-section $\frac{d\sigma}{dE_T^\gamma}$.

E_T^γ range (GeV)	$\frac{d\sigma}{dE_T^\gamma}$ (pb GeV ⁻¹)
4–6	4.87 ± 0.28 (stat.) ^{+0.40} _{-0.23} (syst.)
6–8	2.40 ± 0.16 (stat.) ^{+0.09} _{-0.11} (syst.)
8–10	1.24 ± 0.11 (stat.) ^{+0.03} _{-0.04} (syst.)
10–15	0.55 ± 0.04 (stat.) ^{+0.03} _{-0.03} (syst.)

Table 2Measured differential cross-section $\frac{d\sigma}{d\eta^\gamma}$.

η^γ range	$\frac{d\sigma}{d\eta^\gamma}$ (pb)
-0.7–-0.3	17.4 ± 0.9 (stat.) ^{+0.5} _{-0.7} (syst.)
-0.3–-0.1	13.0 ± 0.8 (stat.) ^{+0.6} _{-0.3} (syst.)
0.1–0.5	10.7 ± 0.9 (stat.) ^{+0.7} _{-0.4} (syst.)
0.5–0.9	8.7 ± 0.9 (stat.) ^{+1.1} _{-0.7} (syst.)

Table 3Measured differential cross-section $\frac{d\sigma}{dQ^2}$.

Q^2 range (GeV ²)	$\frac{d\sigma}{dQ^2}$ (pb GeV ⁻²)
10–20	0.414 ± 0.035 (stat.) ^{+0.045} _{-0.024} (syst.)
20–40	0.279 ± 0.020 (stat.) ^{+0.005} _{-0.014} (syst.)
40–80	0.115 ± 0.008 (stat.) ^{+0.011} _{-0.004} (syst.)
80–150	0.050 ± 0.003 (stat.) ^{+0.001} _{-0.003} (syst.)
150–350	0.0088 ± 0.0009 (stat.) ^{+0.0004} _{-0.0003} (syst.)

Table 4Measured differential cross-section $\frac{d\sigma}{dx}$.

x range	$\frac{d\sigma}{dx}$ (pb)
0.0002–0.001	5560 ± 380 (stat.) ⁺³⁵⁰ ₋₂₅₀ (syst.)
0.001–0.003	3920 ± 230 (stat.) ⁺¹⁵⁰ ₋₁₈₀ (syst.)
0.003–0.01	819 ± 58 (stat.) ⁺⁴⁴ ₋₄₂ (syst.)
0.01–0.02	103 ± 16 (stat.) ⁺¹² ₋₁₆ (syst.)

with an extracted contribution for QQ of

$$12.2 \pm 0.7 \text{ (stat.)}_{-1.0}^{+1.2} \text{ (syst.) pb.}$$

The differential cross sections as functions of E_T^γ , η^γ , Q^2 and x are shown in Fig. 3 and given in Tables 1–4. It can be seen that the cross section decreases with increasing E_T^γ , η^γ , Q^2 and x . The predictions for the sum of the expected LL contribution from DJANGO and a factor of approximately 1.6 times the expected QQ contribution from PYTHIA agree well with the measurements, except for some differences at the lowest Q^2 (and correspondingly lowest x).

The theoretical predictions described in Section 4 are compared to the measurements in Fig. 4. The predictions from GGP describe the shape of the E_T^γ and η^γ distributions well, but their central value typically lies 20% below the measured cross sections. The calculations fail to reproduce the shape in Q^2 ; a similar observation was made by H1 [8]. As with the MC comparison, the measured cross section is larger than the theoretical prediction; this is also reflected in an excess of data over theory at low x .

The MRST predictions mostly fall below the measured differential cross sections. However, they lie close to the measurements at large values of Q^2 and x , for backward η^γ and for high values of E_T^γ , where the LL cross section is expected to be a substantial fraction of the total. Also included in Fig. 4 is the sum of MRST and QQ of GGP; it gives an improved description of the data over much of the range of the kinematic variables.

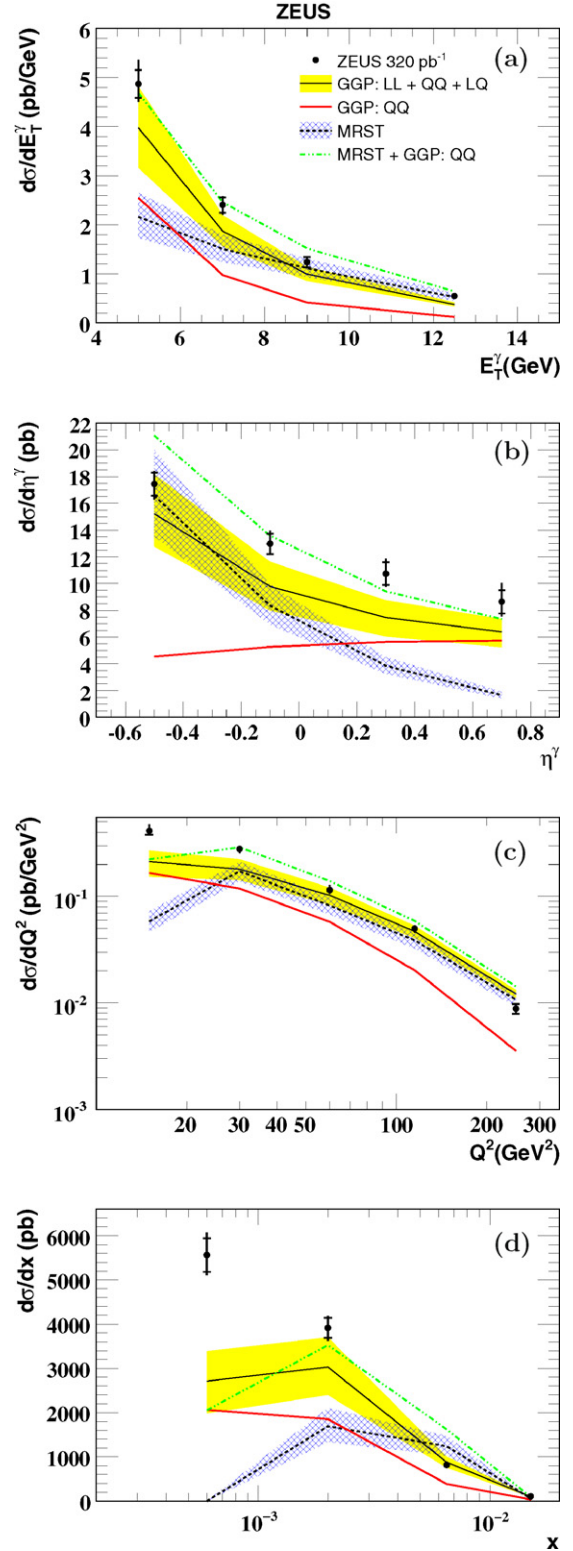


Fig. 4. Data points as Fig. 3. Theoretical predictions from Gehrman-De Ridder et al. and Martin et al. are shown with their associated uncertainties indicated by the shaded band and the hatched bands respectively. The dash-dotted line illustrates the combination MRST plus GGP: QQ.

Fig. 5 shows the measured $d\sigma/d\eta^\gamma$ compared to previous measurements from ZEUS [7] and H1 [8] for the restricted range $Q^2 > 35$ GeV² and $5 < E_T^\gamma < 10$ GeV. The results are consistent but the uncertainty in the present measurement is smaller.

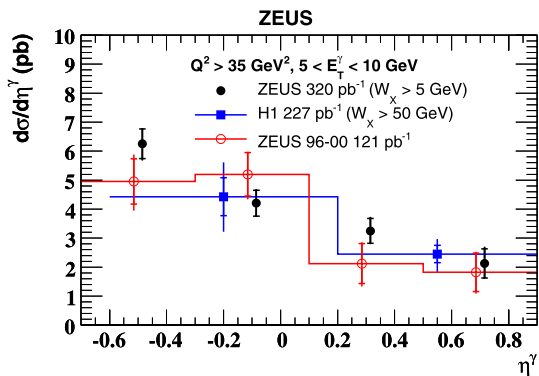


Fig. 5. Isolated photon differential cross-section $\frac{d\sigma}{d\eta^\gamma}$, compared to previous measurements at HERA with the additional kinematic restraints $Q^2 > 35 \text{ GeV}^2$ and $5 < E_T^\gamma < 10 \text{ GeV}$. The histograms show the different binnings used by ZEUS and H1. The symbols are mutually displaced for clarity.

9. Conclusions

Inclusive isolated photon production has been measured in deep inelastic scattering using the ZEUS detector at HERA using an integrated luminosity of 320 pb^{-1} . Differential cross sections as functions of several kinematic variables are presented for $10 < Q^2 < 350 \text{ GeV}^2$ and $W_X > 5 \text{ GeV}$ in the pseudorapidity range $-0.7 < \eta^\gamma < 0.9$ for photon transverse energies in the range $4 < E_T^\gamma < 15 \text{ GeV}$. The order α^3 predictions of Gehrmann-de Ridder et al. reproduce the shapes of the experimental results as functions of transverse energy and pseudorapidity, but are lower than the measurements at low Q^2 and low x . The predictions of Martin et al. mostly fall below the measured cross sections but are close in the kinematic regions where lepton emission is expected to be dominant. An improved description of the data is obtained by appropriately combining the two predictions, suggesting a need for further calculations to exploit the full potential of the measurements.

Acknowledgements

We appreciate the contributions to the construction and maintenance of the ZEUS detector of many people who are not listed as authors. The HERA machine group and the DESY computing staff are especially acknowledged for their success in providing excellent operation of the collider and the data-analysis environment. We thank the DESY directorate for their strong support and encouragement. It is a pleasure to thank T. Gehrmann, W.J. Stirling and R. Thorne for useful discussions.

References

[1] E. Anassontzis, et al., *Z. Phys. C* 13 (1982) 277;

WA70 Collaboration, M. Bonesini, et al., *Z. Phys. C* 38 (1988) 371;
 E706 Collaboration, G. Alverson, et al., *Phys. Rev. D* 48 (1993) 5;
 CDF Collaboration, F. Abe, et al., *Phys. Rev. Lett.* 73 (1994) 2662;
 CDF Collaboration, D. Acosta, et al., *Phys. Rev. Lett.* 95 (2005) 022003;
 DØ Collaboration, B. Abbott, et al., *Phys. Rev. Lett.* 84 (2000) 2786;
 DØ Collaboration, V.M. Abazov, et al., *Phys. Lett. B* 639 (2006) 151.
 [2] ZEUS Collaboration, J. Breitweg, et al., *Phys. Lett. B* 413 (1997) 201.
 [3] ZEUS Collaboration, J. Breitweg, et al., *Phys. Lett. B* 472 (2000) 175.
 [4] ZEUS Collaboration, S. Chekanov, et al., *Phys. Lett. B* 511 (2001) 19.
 [5] ZEUS Collaboration, S. Chekanov, et al., *Eur. Phys. J. C* 49 (2007) 511.
 [6] H1 Collaboration, A. Aktas, et al., *Eur. Phys. J. C* 38 (2004) 437.
 [7] ZEUS Collaboration, S. Chekanov, et al., *Phys. Lett. B* 595 (2004) 86.
 [8] H1 Collaboration, F.D. Aaron, et al., *Eur. Phys. J. C* 54 (2008) 371.
 [9] A. Gehrmann-De Ridder, G. Kramer, H. Spiesberger, *Nucl. Phys. B* 578 (2000) 326.
 [10] A. Gehrmann-De Ridder, T. Gehrmann, E. Poulsen, *Phys. Rev. Lett.* 96 (2006) 132002.
 [11] A. Gehrmann-De Ridder, T. Gehrmann, E. Poulsen, *Eur. Phys. J. C* 47 (2006) 395.
 [12] A.D. Martin, et al., *Eur. Phys. J. C* 39 (2005) 155.
 [13] ZEUS Collaboration, U. Holm (Ed.), *The ZEUS detector. Status report, DESY, 1993* (unpublished), available on <http://www-zeus.desy.de/bluebook/bluebook.html>.
 [14] N. Harnew, et al., *Nucl. Instrum. Meth. A* 279 (1989) 290;
 B. Foster, et al., *Nucl. Phys. Proc. Suppl. B* 32 (1993) 181;
 B. Foster, et al., *Nucl. Instrum. Meth. A* 338 (1994) 254.
 [15] A. Polini, et al., *Nucl. Instrum. Meth. A* 581 (2007) 656.
 [16] M. Derrick, et al., *Nucl. Instrum. Meth. A* 309 (1991) 77;
 A. Andresen, et al., *Nucl. Instrum. Meth. A* 309 (1991) 101;
 A. Caldwell, et al., *Nucl. Instrum. Meth. A* 321 (1992) 356;
 A. Bernstein, et al., *Nucl. Instrum. Meth. A* 336 (1993) 23.
 [17] W.H. Smith, K. Tokushuku, L.W. Wiggers, in: C. Verkerk, W. Wojcik (Eds.), *Proc. Computing in High-Energy Physics (CHEP), Anancy, France, Sept. 1992*, CERN, Geneva, Switzerland, 1992, p. 222. Also in preprint DESY 92-150B;
 P. Allfrey, *Nucl. Instrum. Meth. A* 580 (2007) 1257.
 [18] J. Andruszków, et al., preprint DESY-92-066, DESY, 1992;
 ZEUS Collaboration, M. Derrick, et al., *Z. Phys. C* 63 (1994) 391;
 J. Andruszków, et al., *Acta Phys. Pol. B* 32 (2001) 2025.
 [19] M. Heilbich, et al., *Nucl. Instrum. Meth. A* 565 (2006) 572.
 [20] H. Abramowicz, A. Caldwell, R. Sinkus, *Nucl. Instrum. Meth. A* 365 (1995) 508;
 R. Sinkus, T. Voss, *Nucl. Instrum. Meth. A* 391 (1997) 360.
 [21] ZEUS Collaboration, M. Derrick, et al., *Phys. Lett. B* 303 (1993) 183.
 [22] H1 Collaboration, C. Adloff, et al., *Phys. Lett. B* 517 (2001) 47;
 ZEUS Collaboration, S. Chekanov, et al., *JHEP* 0905 (2009) 108.
 [23] ZEUS Collaboration, J. Breitweg, et al., *Eur. Phys. J. C* 1 (1998) 81;
 ZEUS Collaboration, J. Breitweg, et al., *Eur. Phys. J. C* 6 (1999) 43.
 [24] S. Catani, et al., *Nucl. Phys. B* 406 (1993) 187.
 [25] S.D. Ellis, D.E. Soper, *Phys. Rev. D* 48 (1993) 3160.
 [26] J. Pumplin, et al., *JHEP* 0207 (2002) 012.
 [27] W.J. Stirling, R. Thorne, private communication, 2009.
 [28] T. Gehrmann, private communication, 2009.
 [29] T. Sjöstrand, et al., *JHEP* 0605 (2006) 26.
 [30] K. Charchuła, G.A. Schuler, H. Spiesberger, *Comput. Phys. Commun.* 81 (1994) 381.
 [31] A. Kwiatkowski, H. Spiesberger, H.-J. Möhring, *Comput. Phys. Commun.* 69 (1992) 155.
 [32] L. Lönnblad, *Comput. Phys. Commun.* 71 (1992) 15.
 [33] T. Sjöstrand, *Comput. Phys. Commun.* 39 (1986) 347.
 [34] P.R.B. Saull, GenDVCS 1.0: A Monte Carlo generator for deeply virtual Compton scattering at HERA, 1999, available on <http://www-zeus.desy.de/physics/diff/pub/MC/>.
 [35] T. Abe, *Comput. Phys. Commun.* 136 (2001) 126.
 [36] R. Brun, et al., GEANT3, Technical report CERN-DD/EE/84-1, CERN, 1987.
 [37] M. Forrest, Ph.D. thesis, University of Glasgow, 2010, unpublished.